Lithos 216–217 (2015) 81–92

Contents lists available at ScienceDirect

Lithos

journal homepage: www.elsevier.com/locate/lithos

# Isotopic (Pb, Sr, Nd, C, O) evidence for plume-related sampling of an ancient, depleted mantle reservoir

Wei Chen [a,b,*], Antonio Simonetti [b]

[a] State Key Laboratory of Geological Processes and Mineral Resources, 221 National Lab Building, China University of Geosciences, Wuhan 430074 PR China
[b] Department of Civil & Environmental Engineering & Earth Sciences, 156 Fitzpatrick Hall, University of Notre Dame, Notre Dame IN 46556 USA

ARTICLE INFO

*Article history:*
Received 10 July 2014
Accepted 24 November 2014
Available online 4 December 2014

*Keywords:*
Carbonatite
Alkaline silicate rocks
Radiogenic isotope
Stable isotope
Depleted mantle
Plume

ABSTRACT

The exact mantle source for carbonatite melts remains highly controversial. Despite their predominant occurrence within continental (lithospheric) domains, the radiogenic isotope data from young (<200 Ma) carbonatite complexes worldwide overlap the fields defined by present-day oceanic island basalts (OIBs). This feature suggests an intimate petrogenetic relationship with asthenospheric mantle. New Pb, Sr, C, and O isotopic data are reported here for constituent minerals from the Oka carbonatite complex, which is associated with the Cretaceous Monteregian Igneous Province (MIP), northeastern North America. The Pb isotope data define linear arrays in Pb–Pb isotope diagrams, with the corresponding Sr isotope ratios being highly variable (0.70314–0.70343); both these features are consistent with open system behavior involving at least three distinct mantle reservoirs. Compared to the isotope composition of known mantle sources for OIBs and carbonatite occurrences worldwide, the least radiogenic $^{207}Pb/^{204}Pb$ (14.96 ± 0.07) and $^{208}Pb/^{204}Pb$ (37.29 ± 0.15) isotopic compositions relative to their corresponding $^{206}Pb/^{204}Pb$ ratios (18.86 ± 0.08) reported here are distinct, and indicate the involvement of an ancient depleted mantle (ADM) source. The extremely unradiogenic Pb isotope compositions necessitate U/Pb fractionation early in Earth's history (prior to 4.0 Ga ago) and growth via a multi-stage Pb evolution model. The combined stable (C and O) and radiogenic isotopic compositions effectively rule out crustal/lithosphere contamination during the petrogenetic history of the Oka complex. Instead, the isotopic variations reported here most likely result from the mixing of discrete, small volume partial melts derived from a heterogeneous plume source characterized by a mixed HIMU–EM1–ADM signature.



## 1. Introduction

Radiogenic isotope compositions of the Earth's mantle exhibit large-scale heterogeneities (e.g., Hofmann, 1997), but the origin and distribution of the compositional variations remain unresolved. Four mantle components, i.e., DMM (depleted MORB-mid-ocean ridge basaltic mantle), EM1 (enriched mantle 1), EM2 (enriched mantle 2), and HIMU (high μ (mu) = $^{238}U/^{204}Pb$), have been identified based on the Nd, Pb, and Sr isotope data for OIBs (oceanic island basalts) and MORBs (Zindler and Hart, 1986). Additional mantle reservoirs, FOZO (focus zone) and "C", have been recognized on the basis of unique Pb and He isotope compositions (Hanan and Graham, 1996; Hart et al., 1992).

Compared to their silicate (e.g., basaltic) counterparts, mantle-derived carbonatitic melts hold several advantages as insightful probes into the elemental and isotopic nature of the Earth's mantle. Their low melt viscosities result in rapid ascent rates through the lithosphere and crust (Treiman, 1989), and their enrichment in incompatible elements (e.g., Nd, Sr) results in minimal contamination and perturbation of their inherited mantle source isotopic signatures (e.g., Bell and Simonetti, 2010; Bell and Tilton, 2001). For example, Bell et al. (1982) advocated for the existence of a long-lived, time-integrated depleted upper mantle reservoir beneath eastern North America on the basis of Sr isotope signatures for Canadian carbonatites varying in age range between ~2.7 and ~0.1 Ga. Additionally, Bizzarro et al. (2002) reported the existence of an unradiogenic mantle reservoir preserved in the deep mantle for at least 3 b.y. based on Hf isotopic results for carbonatites and kimberlites from Greenland and eastern North America.

A considerable amount of radiogenic and stable isotope data for carbonatites and associated alkaline silicate rocks has been reported within the last 20 years (e.g., Andersen and Taylor, 1988; Bell, 1998; Grünenfelder et al., 1986; Simonetti and Bell, 1994; Tilton and Bell, 1994). However, various interpretations/models have been put forward to explain the origin of the associated alkaline silicate rocks, and these include: 1) low degrees partial melting of a metasomatized upper mantle (e.g., Olafsson and Eggler, 1983); 2) fractional crystallization from a homogeneous, mantle-derived melt in a closed system (e.g., Balaganskaya et al., 2007; Brassinnes et al., 2005); 3) liquid immiscibility between a carbonatitic melt and a conjugate parental alkaline silicate magma

* Corresponding author at: State Key Laboratory of Geological Processes and Mineral Resources, 221 National Lab Building, China University of Geosciences, Wuhan 430074 PR China. Tel./fax: +86 027 67885096.
*E-mail addresses:* wchencug@163.com (W. Chen), simonetti.3@nd.edu (A. Simonetti).

http://dx.doi.org/10.1016/j.lithos.2014.11.024
0024-4937/

(e.g., Ivanikov et al., 1998); 4) rheomorphism of fenites at crustal levels, in particular for rocks of ijolitic and syenitic composition (e.g., Kramm, 1994).

The Cretaceous Oka carbonatite complex within southern Québec (Canada) contains both carbonatite and associated alkaline silicate rocks (e.g., alnoite, ijolite), and is the most westerly alkaline intrusive center associated with the Monteregian Igneous Province (MIP; Fig. 1). Recent, detailed in-situ U/Pb geochronological investigations of apatite, niocalite, and perovskite reveal that the magmatic activity (maximum extent) at Oka was a prolonged event, which occurred between 109.9 ± 2.7 and 139.9 ± 2.5 Ma ago (Chen and Simonetti, 2013, 2014; Chen et al., 2013b). Treimain and Essene (1985) proposed that the carbonatite and associated silicate rocks (i.e., okaite, ijolite) were derived from a common primary magma and formed via liquid immiscibility. In contrast, on the basis of U–Pb ages, major and trace element geochemistry, and radiogenic isotope data, Chen & Simonetti (2013, 2014) and Chen et al. (2013b) suggested that the carbonatites and associated alkaline silicate rocks are the result of open system behavior involving mixing of different pulses of small volume partial melts. Previous investigations have attributed the origin of the MIP-related alkaline plutons to melting of lithospheric mantle at the time of the opening of the North Atlantic Ocean (Faure et al., 1996), or of mantle plume origin (Eby, 1985; Foland et al., 1988; Roulleau and Stevenson, 2013). The MIP has also been linked to the intrusions of the New Hampshire White Mountains and the New England seamount chain as expressions of the Great Meteor hotspot track (Fig. 1a; Eby, 1985; Foland et al., 1988; Heaman and Kjarsgaard, 2000; Zurevinski et al., 2011).

This study reports new, in-situ Sr, Nd and Pb isotopic compositions of calcite and apatite from both carbonatite and associated silicate rocks at Oka. Previous investigations report the major and trace element compositions and U–Pb ages for apatite, niocalite, and perovskite (Chen and Simonetti, 2013, 2014; Chen et al., 2013b), and the composition of melt inclusions within magnetite (Chen et al., 2013a) for carbonatite and associated silicate rocks investigated here. The stable $\delta^{13}C$ and $\delta^{18}O$ values for calcite are also documented, which constrain the nature of the mantle sources involved in the generation of the Oka complex. The combined stable and radiogenic isotope data help delineate the petrogenetic relationship between the carbonatites and associated alkaline silicate rocks at Oka, and more importantly, the mantle sources that contribute to the generation of Oka and MIP-related intrusions.

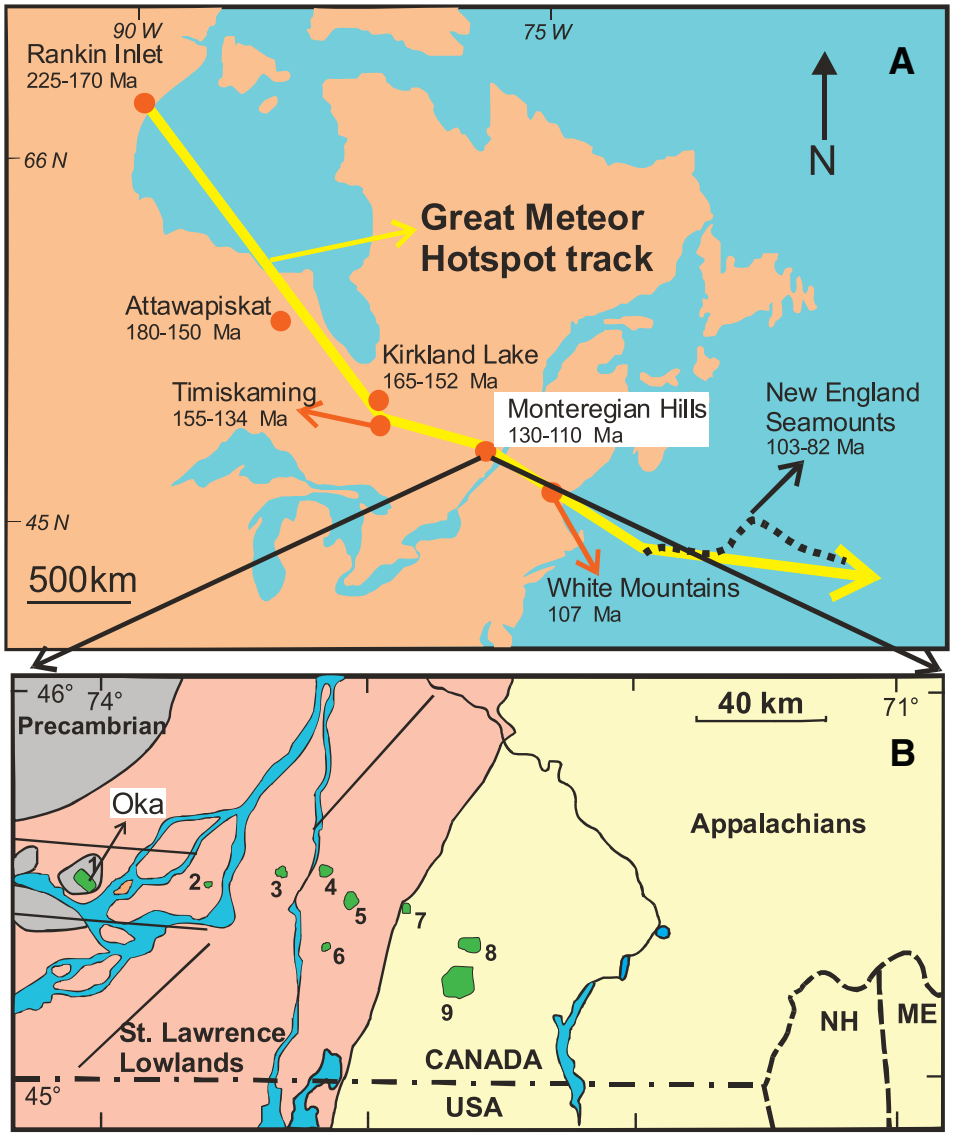


**Fig. 1.** Map of eastern North America showing the Great Meteor hotspot track (A; Heaman and Kjarsgaard, 2000; Zurevinski et al., 2011), and inset (B) illustrates the location of MIP-related intrusions including Oka (Chen and Simonetti, 2013; Faure et al., 1996); MIP-related intrusions labeled in inset (B) are: 2 — Royal; 3 — Bruno; 4 — St. Hilaire; 5 — Rougemont; 6 — Johnson; 7 — Yamaska; 8 — Shefford; 9 — Brome.

## 2. Sample descriptions and petrography

The Oka carbonatite complex is one of the youngest carbonatite occurrences in North America, and was mined for Nb (pyrochlore) at three localities — St. Lawrence Columbium Deposit, the Bond Zone, and the NIOCAN deposit (Fig. 2). Oka contains both carbonatite and associated silicate rocks, the latter includes okaite, calcitic ijolite, ijolite, alnoite and jacupirangite (Fig. 3). In total, ~50 samples were collected from four locations marked on the map (Stops 1.4, 2.2, 2.3, 2.4; Fig. 2), and correspond to those outlined in the 1986 GAC-MAC-sponsored Oka field excursion (Gold et al., 1986). The samples selected for this investigation consist of 13 carbonatites, 4 okaites from Husereau Hill (Stop 2.3), 3 calcitic ijolites and 1 ijolite from Stop 2.2, and both the alnoites and jacupirangites were retrieved from the Bond Zone area (Stop 2.4). The following sample descriptions are summarized from Chen and Simonetti (2013). Coarse-grained carbonatites contain accessory apatite, biotite, monticellite, oxides and lack pyrochlore (Fig. 3a). Calcitic ijolite is the dominant rock type in Stop 2.2, which is also located in the southern ring, and consists predominantly of clinopyroxene, nepheline, melanite, calcite, and accessory apatite (Fig. 3b). Stop 2.3 is located in the Husereau Hill area within the northern ring (Fig. 2), and it is the type locality for okaite. The latter is a melilite-bearing rock, with accessory calcite, apatite, biotite, perovskite, and other oxides (e.g., Fig. 3c); examples include samples Oka137, Oka138 and Oka229. Olivine, augite, and biotite are the dominant phenocrysts in alnoite, with magnetite, melilite, calcite, melanite, apatite, and perovskite present as phases in the surrounding matrix (Fig. 3e). Jacupirangite from the Bond Zone consists predominantly of augite (~60–70%) and nepheline (20–15%) with minor magnetite, apatite, biotite, calcite, and perovskite (Fig. 3f).

Prior to isotopic analysis, all samples investigated here were examined petrographically (e.g., Fig. 3), and major element compositions were determined by electron microprobe analysis and scanning electron microscopy; in-situ trace element abundances using petrographic thin sections were obtained by laser ablation-inductively coupled plasma mass spectrometry (LA-ICP-MS; e.g., Chen et al., 2013b; Chen and Simonetti, 2013, 2014); moreover, in-situ U–Pb ages for several mineral phases (apatite, niocalite, perovskite- Chen et al., 2013b; Chen and Simonetti, 2013, 2014) were reported for the same samples investigated here. Overall, mineral grains selected for analysis in this study were medium-to-coarse-grained in size and large enough for in-situ isotope analysis (i.e., >100 μm), and typically "fresh" in nature, i.e., lack textural evidence for secondary alteration (Fig. 3).

## 3. Analytical methods

In-situ common Pb isotope compositions for calcite, melilite, and nepheline were determined using a NWR193 nm laser ablation system coupled to a Nu Plasma II MC-ICP-MS instrument at the MITERAC facility, University of Notre Dame. Mineral grains were analyzed in line raster mode using a 150 μm spot size, 7–12 Hz repetition rate, and an energy density ~ 10–12 J/cm$^2$. Data reduction involved using a 45 s 'on-peak' blank measurement and the Time Resolved Analysis (TRA) software from Nu Instruments. Blocks of analyses consisted of 6 unknowns that were bracketed by repeated measurement (n = 4) of the NIST SRM 614 standard (Pb isotope values from Baker et al., 2004) in order to monitor for instrumental mass bias and instrument drift (e.g., Bellucci et al., 2013). For several larger (individual) calcite grains (>300 μm), more than one laser ablation analysis was conducted in order to investigate the isotopic homogeneity. Individual analyses that yielded <40 mV of $^{208}$Pb ion signal are not reported here consequently due to the extremely low ion signal for $^{204}$Pb. In general, the external reproducibility of the $^{204}$Pb-normalized ratios obtained for the NIST SRM 614 standard during the multiple analytical sessions approximates that of the typical errors associated with the individual $^{206}$Pb/$^{204}$Pb, $^{207}$Pb/$^{204}$Pb, and $^{208}$Pb/$^{204}$Pb ratio measurements (Table 1), which is ~0.3%, ~ 0.3%, and ~0.6% (relative standard deviation at 2σ level), respectively. The accuracy and validation of the analytical protocol was evaluated with repeated analysis of an amazonite feldspar in-house standard from the Broken Hill deposit, Australia (along with measurement of the NIST SRM 612 standard). The average Pb isotope values obtained for the amazonite feldspar are indistinguishable from those previously reported by TIMS (thermal ionization mass spectrometry) measurement (Gulson, 1984), and LA-MC-ICP-MS for the ore and feldspar from the Broken Hill deposit (Schmidberger et al., 2007), respectively.

In-situ Sr isotope ratios for calcite (and some clinopyroxene and nepheline) were determined with the same instrument configuration described above. The measurements involve correction of critical spectral interferences that include Kr, Rb, and doubly charged Rare Earth elements (REEs; e.g., Paton et al., 2007; Ramos et al., 2004). These detailed corrections are adopted in this study and are identical to those reported in Chen et al. (2013b) and Chen and Simonetti (2014). A modern-day

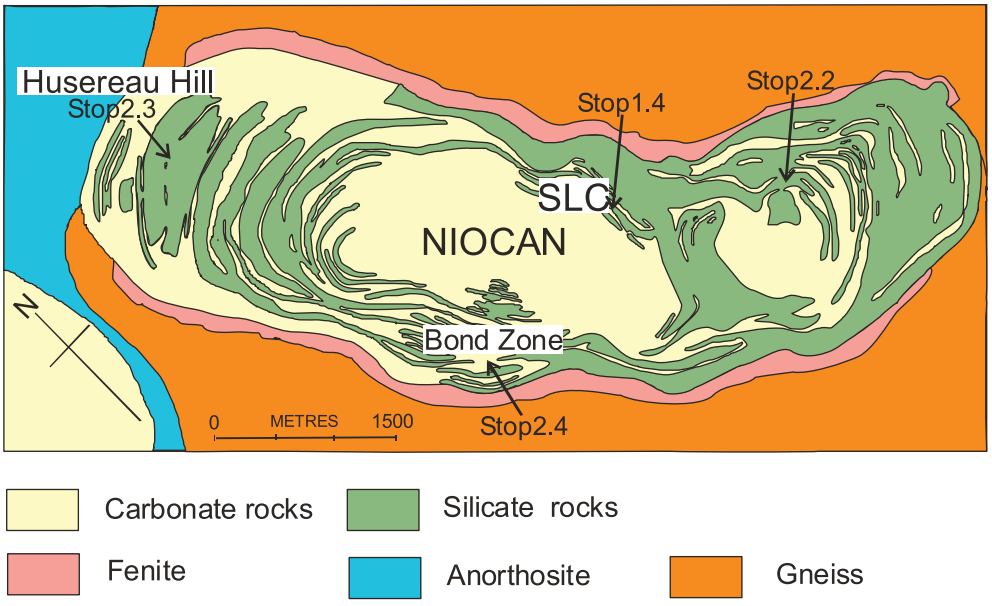


**Fig. 2.** Geological map of the Oka carbonatite complex (after Chen and Simonetti, 2013, 2014; Gold et al., 1986). Sample stop numbers correspond to those from 1986 GAC-MAC-sponsored Oka field excursion (Gold et al., 1986).

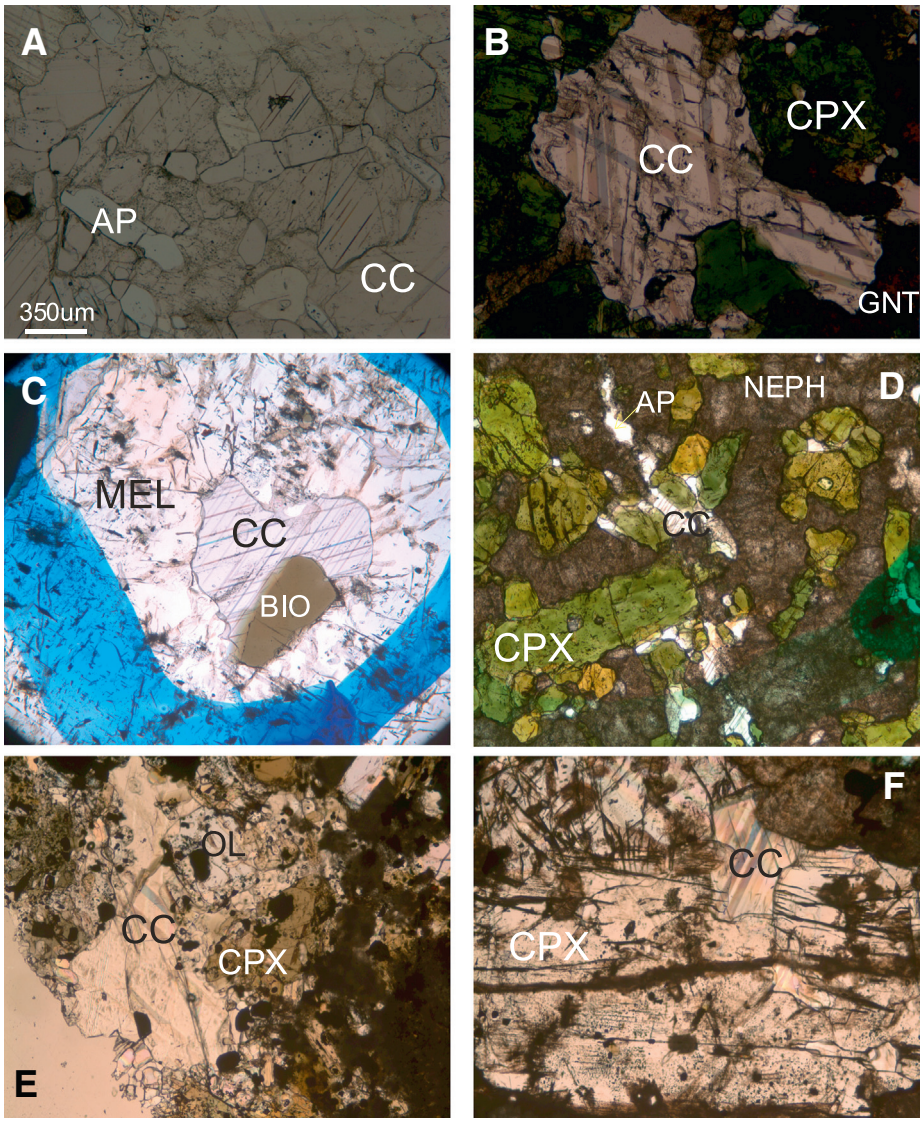


**Fig. 3.** Petrographic photomicrographs illustrating the mineralogy of the different rock types investigated here. (A) carbonatite — Oka200a; (B) calcitic ijolite — Oka21; (C) okaite — Oka137; (D) ijolite — Oka88; (E) alnoite — Oka73; (F) jacupirangite — Oka70. CC: calcite; AP: apatite; BIO: biotite; CPX: clinopyroxene; GNT: garnet; MEL: melilite; NEPH: nepheline; OL: olivine. Scale for photomicrographs is identical to that shown in 3A.

coral (Indian Ocean) served as an external, in-house standard, which is well characterized for its $^{87}Sr/^{86}Sr$ isotopic composition by ID-TIMS (Bizzarro et al., 2003). The coral standard and calcite grains were analyzed using either a 75 or 100 μm spot size depending on the Sr abundances, 7 Hz repetition rate, and an energy density ~11 J/cm$^2$. The average $^{87}Sr/^{86}Sr$ ratio obtained for the coral standard is 0.70910 ± 0.00001 based on 20 measurements (Table 2), and is indistinguishable (within error) to the corresponding TIMS value of 0.70910 ± 0.00002 (Bizzarro et al., 2003). For the calcite from Oka, Rb concentrations are close to or below the detection limit obtained for in-situ LA-ICP-MS analyses (i.e., <<1 ppm; Chen and Simonetti, 2013), and consequently the calculated Rb/Sr ratios are low since Sr abundances are extremely high (in general >10,000 ppm; Chen and Simonetti, 2013) such that the magnitude of the age correction on the measured $^{87}Sr/^{86}Sr$ ratio is negligible given the relatively young age of the complex. The analytical protocol used for determining the in-situ Nd isotope ratios of individual apatite grains is described in Chen and Simonetti (2014).

Carbon and oxygen isotope analysis of calcite was performed using the conventional orthophosphoric acid digestion method (McCrea, 1950). Approximately 1 mg of carbonate sample powder and ~ 0.5 ml of concentrated $H_3PO_4$ ("104%") were placed in sealed tubes and thermally equilibrated at 100 °C, and reacted for >1 h. The isotope compositions were subsequently determined using a Delta V Advantage isotope ratio mass spectrometer at the Center for Environmental Science and Technology (CEST), University of Notre Dame. Carbon and oxygen isotope data are reported in per mil notation (‰) using standard δ notation as $\delta^{13}C$ and $\delta^{18}O$ values relative to standard mean ocean water (SMOW; Coplen et al., 1983) and Peedee belemnite (PDB; Craig, 1961), respectively. Analysis of standard NBS 19 yielded C and O isotopic ratios identical to certified values ($\delta^{13}C$ = 1.95‰, $\delta^{18}O$ = 28.65‰; Coplen et al., 1983, 2006).

## 4. Geochemical results

### 4.1. Sr, Pb, and Nd isotopic compositions

The new in-situ Pb isotope data are presented in Table 1 and Fig. 4, which were obtained at high spatial resolution by laser ablation-multicollector-inductively coupled plasma mass spectrometry (LA-MC-ICP-MS) for constituent magmatic minerals (calcite, melilite, and nepheline) of various alkaline rocks from Oka. Overall, as reported in

Chen and Simonetti (2013), U concentrations in calcite are below (or close to) detection limit (<<0.01 ppm) obtained for in-situ LA-ICP-MS. As a result, the U/Pb ratios are extremely small so that the age correction for the Pb isotopic ratios is negligible (i.e., typically within the associated analytical uncertainty) given the relatively young age of the Oka complex.

In total, ~70 grains were analyzed for their Pb isotope compositions from 13 carbonatites, 4 okaites, 3 calcitic ijolites, 2 alnoites, and 2 jacupirangites. The Pb isotopic compositions for carbonatites define a wide range of values for the $^{206}Pb/^{204}Pb$ (18.86–20.24), $^{207}Pb/^{204}Pb$ (14.96–15.86), and $^{208}Pb/^{204}Pb$ (37.29–40.28) ratios (Table 1). Most of the okaites and alnoites are characterized by a more radiogenic Pb isotope signature, whereas those for calcitic ijolite and jacupirangite show a large variation in Pb isotope compositions (Table 1). In addition, duplicate analyses within the same grain indicate isotopic homogeneity since the Pb isotope ratios are indistinguishable given their associated errors as shown in Table 1 (e.g., Oka51 CC2 & CC2_2). The Pb isotope compositions are shown in Fig. 4 along with the Pb isotope ratios obtained by solution mode MC-ICP-MS analysis for mineral separates (plagioclase) from MIP-related intrusions (Roulleau and Stevenson, 2013; Roulleau et al., 2012). The field for carbonatite complexes worldwide illustrated in Fig. 4 is defined by Pb isotope data for oceanic carbonatites (e.g., Hoernle et al., 2002) and carbonatites from different continents (e.g., Bell and Simonetti, 1996; Bell and Tilton, 2001; Bizimis et al., 2003; Hoernle et al., 2002; Kalt et al., 1997; Paslick et al., 1995; Tappe et al., 2007; Tilton and Bell, 1994; Tilton et al., 1987; Toyoda et al., 1994; Xu et al., 2011). It is clear that a significant number of the Pb isotopic compositions (i.e., those with the least radiogenic $^{207}Pb/^{204}Pb$ and $^{208}Pb/^{204}Pb$ ratios) for Oka and MIP-related centers are quite distinct compared to those for carbonatite complexes worldwide (Fig. 4a&b). In particular, the former are characterized by large variations for the $^{207}Pb/^{204}Pb$ (14.96–15.99) and $^{208}Pb/^{204}Pb$ (37.29–40.28) ratios relative to their associated $^{206}Pb/^{204}Pb$ values.

The new in-situ Sr isotopic data for calcite from carbonatite, okaite, calcitic ijolite, alnoite, and jacupirangite are given in Table 2 and shown in Fig. 5. As discussed earlier, the $^{87}Rb/^{86}Sr$ ratio for calcite is extremely low given the insignificant Rb concentrations and very high Sr abundances, and consequently the age correction for the measured $^{87}Sr/^{86}Sr$ ratios is negligible (i.e., typically within the associated analytical uncertainty). $^{87}Sr/^{86}Sr$ ratios for ~50 calcite grains define a range of values from 0.70314 to 0.70343 (Fig. 5a; Table 2), which overlaps the entire range defined by previously reported whole rock isotope data (Wen et al., 1987). Calcite from carbonatites and the associated silicate rocks define a similar range of Sr isotope values (Table 2). In addition, the Sr isotope ratios for calcite are similar (given their associated uncertainties) to those for corresponding apatite from the same sample (i.e., plot proximal to the 1:1 line in Fig. 5b; each point represents the weighted average of the Sr isotope ratio for calcite and apatite for each sample). The Sr and Pb isotopic ratios for both carbonatite and associated silicate rocks are highly variable (Fig. 5a), and both groups display a similar range of values (Figs. 4 & 5a). Lastly, in-situ Nd isotope ratios were measured for apatite from carbonatite and associated silicate rocks (Chen and Simonetti, 2014), which vary between ~0.51275 and ~0.51285, and do not indicate trends with either their corresponding Sr (for apatite, calcite) or Pb (for calcite) isotope ratios from the same sample.

### 4.2. C and O isotopes

New C and O stable isotope ratio measurements have been obtained for calcite separates from a variety of carbonatites and associated silicate rocks (okaite and calcitic ijolite), and these are listed in Table 3 and displayed in Fig. 6. The $\delta^{18}O$ and $\delta^{13}C$ values for carbonates from Oka carbonatite, okaite, and calcitic ijolite define a range of 6.09–9.76‰ and −4.56 ~ −6.32‰, respectively. As shown in Fig. 6, stable isotope compositions obtained here overlap the range defined by whole rock data from Denies (1989), and those for carbonatites are identical to the O and C isotope results obtained by Haynes et al. (2003; Fig. 6). Significantly, all of the data lie within the field defined for mantle-derived carbon and oxygen ("mantle box"; Keller and Hoefs, 1995).

## 5. Discussion

### 5.1. Modeling of Pb isotope data — involvement of ancient depleted mantle ('ADM')

The reported Pb isotope ratios define linear arrays (Fig. 4), which are indicative of mixing between at least two mantle source endmembers. The "radiogenic" endmember may be attributed to derivation of carbonatite and associated alkaline silica-undersaturated melts from a mantle source region characterized by a mixed HIMU–EM1 isotopic signature; such a model has been proposed for the carbonatite-alkaline magmatism associated with the East African Rift (Bell and Simonetti, 2010; Bell and Tilton, 2001). Unlike the majority of carbonatite complexes worldwide, which typically involve HIMU and EM1 mantle components within their mantle source regions (e.g., Bell, 1998; Bell and Simonetti, 2010; Simonetti and Bell, 1994; Tilton and Bell, 1994), the required Pb isotope composition for the "unradiogenic" endmember of the Oka-MIP mixing array (i.e., the least radiogenic $^{207}Pb/^{204}Pb$ and $^{208}Pb/^{204}Pb$ with moderate $^{206}Pb/^{204}Pb$) in Fig. 4 cannot be attributed to the involvement of either HIMU, EM1, EM2, DMM, FOZO, or "C" mantle components.

The extremely depleted $^{207}Pb/^{204}Pb$ and $^{208}Pb/^{204}Pb$ ratios reported here suggest that the MIP-related alkaline magmatism records the involvement of ancient depleted mantle (ADM). Assuming a mantle origin, such significantly depleted Pb isotopic ratios must be attributed to the fractionation of U vs. Pb early in Earth's history, probably during core formation (e.g., Dupré and Allègre, 1980). The relatively short half-life (0.70 Ga) of $^{235}U$ renders the $^{207}Pb/^{204}Pb$ ratios sensitive to U:Pb differentiation processes that occurred prior to *ca.* 2.5 Ga ago (Halliday et al., 1992; Kwon et al., 1989); in contrast the longer half-life (4.47 Ga) of $^{238}U$ yields $^{206}Pb/^{204}Pb$ ratios that record U:Pb fractionation events at any time during Earth's history (Halliday et al., 1992; Kwon et al., 1989). Similarly, on a Sr vs. Pb isotope plot (Fig. 5c), the isotopic data may be attributed to the mixing of three mantle endmembers, including HIMU, EM1, and 'ADM'. However, it is difficult to constrain exactly the Sr isotopic composition of the ADM component in Fig. 5 since ~2.7 Ga old seawater-altered oceanic crust will be characterized by a $^{87}Sr/^{86}Sr \approx 0.702$ (Ray et al., 2002; Shields and Veizer, 2001), assuming that the ADM represents an ancient, subducted component. However, as described below, the ADM component also underwent metasomatic enrichment at ~2.7 Ga, which may have subsequently increased its $^{87}Sr/^{86}Sr$.

All of the Pb isotope data for the Oka-MIP association plot to the right of the Geochron indicating derivation from a mantle source with an elevated time-integrated μ ($^{238}U/^{204}Pb$) ratio (relative to bulk Earth; Fig. 4a). However, in order to generate the proposed unradiogenic $^{207}Pb/^{204}Pb$ composition for the ADM (Fig. 7), a multi-stage Pb growth evolution must be invoked. In the first stage, the ADM evolved from 4.56 Ga with a $\mu = 7.192$ (equivalent to Bulk Earth) to either ~4.3 or ~4.0 Ga ago when an important chemical differentiation event occurred. The latter has been proposed based on Nd and Hf isotopic results from juvenile rocks worldwide (Bizzarro et al., 2002; Collerson et al., 1991; Vervoort and Blichert-Toft, 1999). Consequently, the second stage of the proposed Pb isotope model for the ADM began at either ~4.3 or ~4.0 Ga and continued to evolve with lower μ value (~4.5) until ~2.7 Ga. In the third stage, at 2.7 Ga the ADM experienced (metasomatic) enrichment and evolved to the main period of Oka-related magmatism (between ~115 and ~127 Ma; Chen and Simonetti, 2013) with a μ ~12.5. At ~2.7 Ga ago, this period in Earth's history is marked by active tectonism and volcanism (e.g., Archean greenstone belts) and is a major episode of crust formation in North America

**Table 1**
In-situ Pb isotopic compositions for calcite, melilite, and nepheline associated with the Oka carbonatite complex, Québec, Canada.

| Sample | Rock types | Analysis No. | $^{206}Pb/^{204}Pb$ | $2\sigma_{(mean)}$ | $^{207}Pb/^{204}Pb$ | $2\sigma_{(mean)}$ | $^{208}Pb/^{204}Pb$ | $2\sigma_{(mean)}$ | $^{207}Pb/^{206}Pb$ | $2\sigma_{(mean)}$ | $^{208}Pb/^{206}Pb$ | $2\sigma_{(mean)}$ |
|---|---|---|---|---|---|---|---|---|---|---|---|---|
| Oka51 | Carb. | CC2 | 19.58 | 0.09 | 15.55 | 0.07 | 38.99 | 0.18 | 0.7928 | 0.0012 | 1.9865 | 0.0019 |
| | | CC2_2 | 19.69 | 0.11 | 15.64 | 0.09 | 39.25 | 0.21 | 0.7936 | 0.0007 | 1.9906 | 0.0019 |
| | | CC1 | 19.70 | 0.12 | 15.64 | 0.10 | 39.21 | 0.22 | 0.7927 | 0.0012 | 1.9891 | 0.0027 |
| | | CC8 | 19.57 | 0.08 | 15.57 | 0.07 | 39.07 | 0.18 | 0.7941 | 0.0009 | 1.9927 | 0.0016 |
| Oka92 | Carb. | CC1 | 19.37 | 0.09 | 15.30 | 0.08 | 38.53 | 0.19 | 0.7902 | 0.0007 | 1.9881 | 0.0022 |
| | | CC6 | 19.62 | 0.10 | 15.53 | 0.08 | 39.11 | 0.20 | 0.7905 | 0.0010 | 1.9917 | 0.0019 |
| | | CC6_2 | 19.84 | 0.09 | 15.72 | 0.07 | 39.58 | 0.18 | 0.7916 | 0.0008 | 1.9925 | 0.0014 |
| | | CC4 | 19.58 | 0.08 | 15.50 | 0.06 | 39.03 | 0.15 | 0.7912 | 0.0006 | 1.9918 | 0.0015 |
| Oka109 | Carb. | CC4 | 19.20 | 0.04 | 15.31 | 0.03 | 38.17 | 0.07 | 0.7968 | 0.0007 | 1.9846 | 0.0012 |
| | | CC5 | 19.24 | 0.04 | 15.34 | 0.04 | 38.25 | 0.09 | 0.7967 | 0.0004 | 1.9878 | 0.0011 |
| | | CC8 | 19.32 | 0.03 | 15.36 | 0.02 | 38.23 | 0.05 | 0.7945 | 0.0003 | 1.9773 | 0.0009 |
| | | CC9 | 19.26 | 0.03 | 15.33 | 0.02 | 38.18 | 0.05 | 0.7948 | 0.0004 | 1.9804 | 0.0008 |
| | | CC12 | 19.33 | 0.03 | 15.38 | 0.02 | 38.36 | 0.06 | 0.7953 | 0.0005 | 1.9819 | 0.0008 |
| Oka200a | Carb. | CC2 | 19.38 | 0.03 | 15.41 | 0.03 | 38.51 | 0.06 | 0.7946 | 0.0005 | 1.9853 | 0.0010 |
| | | CC4 | 19.45 | 0.07 | 15.47 | 0.05 | 38.61 | 0.05 | 0.7953 | 0.0008 | 1.9850 | 0.0020 |
| | | CC5 | 19.41 | 0.05 | 15.45 | 0.04 | 38.57 | 0.10 | 0.7956 | 0.0007 | 1.9851 | 0.0017 |
| Oka200b | Carb. | CC1 | 19.85 | 0.07 | 15.75 | 0.05 | 39.47 | 0.13 | 0.7932 | 0.0007 | 1.9883 | 0.0013 |
| | | CC2 | 19.82 | 0.06 | 15.73 | 0.04 | 39.37 | 0.10 | 0.7936 | 0.0006 | 1.9871 | 0.0015 |
| | | CC7 | 19.86 | 0.07 | 15.74 | 0.05 | 39.43 | 0.13 | 0.7928 | 0.0007 | 1.9881 | 0.0017 |
| | | CC8 | 19.82 | 0.05 | 15.71 | 0.04 | 39.39 | 0.11 | 0.7931 | 0.0008 | 1.9895 | 0.0018 |
| | | CC10 | 19.79 | 0.06 | 15.69 | 0.04 | 39.35 | 0.01 | 0.7926 | 0.0006 | 1.9887 | 0.0012 |
| | | CC11 | 19.84 | 0.06 | 15.73 | 0.04 | 39.43 | 0.11 | 0.7929 | 0.0005 | 1.9896 | 0.0016 |
| Oka200c | Carb. | CC2 | 19.43 | 0.06 | 15.45 | 0.04 | 38.64 | 0.10 | 0.7947 | 0.0009 | 1.9868 | 0.0017 |
| | | CC5 | 19.41 | 0.05 | 15.45 | 0.05 | 38.54 | 0.10 | 0.7949 | 0.0007 | 1.9834 | 0.0016 |
| | | CC11 | 19.41 | 0.05 | 15.43 | 0.03 | 38.51 | 0.09 | 0.7948 | 0.0005 | 1.9835 | 0.0009 |
| Oka4a | Carb. | CC2 | 19.18 | 0.08 | 15.15 | 0.07 | 37.96 | 0.16 | 0.7906 | 0.0009 | 1.9777 | 0.0021 |
| | | CC7 | 19.25 | 0.09 | 15.29 | 0.07 | 38.20 | 0.18 | 0.7941 | 0.0008 | 1.9833 | 0.0013 |
| | | CC10 | 19.42 | 0.08 | 15.42 | 0.07 | 38.49 | 0.20 | 0.7931 | 0.0008 | 1.9803 | 0.0021 |
| | | CC13_2 | 19.18 | 0.07 | 15.18 | 0.05 | 37.94 | 0.13 | 0.7914 | 0.0008 | 1.9783 | 0.0019 |
| Oka4b | Carb. | CC1_2 | 19.19 | 0.09 | 15.25 | 0.07 | 37.99 | 0.19 | 0.7946 | 0.0008 | 1.9834 | 0.0015 |
| | | CC2 | 18.86 | 0.08 | 14.96 | 0.07 | 37.29 | 0.15 | 0.7930 | 0.0012 | 1.9775 | 0.0012 |
| | | CC4_2 | 19.38 | 0.11 | 15.37 | 0.09 | 38.46 | 0.21 | 0.7907 | 0.0009 | 1.9822 | 0.0020 |
| | | CC6 | 19.59 | 0.11 | 15.55 | 0.09 | 38.95 | 0.22 | 0.7926 | 0.0008 | 1.9867 | 0.0018 |
| Oka72 | Carb. | CC8 | 19.25 | 0.16 | 15.27 | 0.11 | 38.43 | 0.31 | 0.7905 | 0.0015 | 1.9897 | 0.0026 |
| Oka144 | Carb. | CC4 | 19.46 | 0.13 | 15.44 | 0.09 | 38.60 | 0.24 | 0.7919 | 0.0012 | 1.9813 | 0.0011 |
| | | CC6 | 19.37 | 0.17 | 15.39 | 0.14 | 38.43 | 0.34 | 0.7918 | 0.0013 | 1.9821 | 0.0021 |
| | | CC7 | 19.39 | 0.14 | 15.40 | 0.09 | 38.48 | 0.26 | 0.7929 | 0.0015 | 1.9827 | 0.0015 |
| | | CC11 | 19.60 | 0.13 | 15.52 | 0.10 | 38.86 | 0.29 | 0.7923 | 0.0009 | 1.9847 | 0.0017 |
| Oka153 | Carb. | CC9 | 20.07 | 0.10 | 15.90 | 0.08 | 39.96 | 0.18 | 0.7919 | 0.0007 | 1.9897 | 0.0022 |
| | | CC14 | 19.74 | 0.09 | 15.71 | 0.07 | 39.54 | 0.17 | 0.7940 | 0.0014 | 2.0009 | 0.0020 |
| Oka203 | Carb. | CC1 | 20.24 | 0.12 | 15.99 | 0.09 | 40.28 | 0.21 | 0.7896 | 0.0010 | 1.9865 | 0.0020 |
| | | CC1_2 | 19.89 | 0.12 | 15.71 | 0.09 | 39.57 | 0.23 | 0.7900 | 0.0005 | 1.9889 | 0.0020 |
| | | CC3 | 19.81 | 0.09 | 15.68 | 0.06 | 39.41 | 0.17 | 0.7908 | 0.0010 | 1.9879 | 0.0013 |
| | | CC4 | 19.99 | 0.13 | 15.86 | 0.12 | 39.78 | 0.28 | 0.7911 | 0.0009 | 1.9891 | 0.0023 |
| Oka206 | Carb. | CC7 | 19.61 | 0.01 | 15.50 | 0.06 | 38.76 | 0.15 | 0.7920 | 0.0011 | 1.9787 | 0.0016 |
| | | CC_Spot10 | 19.42 | 0.08 | 15.40 | 0.09 | 38.41 | 0.15 | 0.7926 | 0.0009 | 1.9778 | 0.0016 |
| | | NEPH_Spot5 | 19.50 | 0.06 | 15.36 | 0.05 | 38.54 | 0.11 | 0.7872 | 0.0009 | 1.9762 | 0.0017 |
| Oka137 | Okaite | CC2 | 19.80 | 0.05 | 15.71 | 0.04 | 39.39 | 0.09 | 0.7943 | 0.0004 | 1.9914 | 0.0014 |
| | | CC | 19.71 | 0.08 | 15.64 | 0.06 | 39.28 | 0.14 | 0.7935 | 0.0012 | 1.9900 | 0.0018 |
| | | MEL | 19.80 | 0.03 | 15.73 | 0.03 | 39.41 | 0.07 | 0.7938 | 0.0005 | 1.9894 | 0.0012 |
| | | MEL3 | 19.77 | 0.04 | 15.70 | 0.03 | 39.36 | 0.07 | 0.7933 | 0.0004 | 1.9899 | 0.0009 |
| Oka138 | Okaite | CC1 | 19.45 | 0.08 | 15.45 | 0.08 | 38.99 | 0.18 | 0.7947 | 0.0012 | 2.0050 | 0.0022 |
| | | CC2 | 19.46 | 0.07 | 15.53 | 0.06 | 38.94 | 0.17 | 0.7975 | 0.0008 | 1.9987 | 0.0020 |
| Oka208 | Okaite | MEL1 | 19.75 | 0.08 | 15.68 | 0.06 | 39.28 | 0.15 | 0.7936 | 0.0008 | 1.9884 | 0.0016 |
| | | MEL2 | 19.75 | 0.08 | 15.68 | 0.05 | 39.26 | 0.13 | 0.7936 | 0.0011 | 1.9848 | 0.0033 |
| Oka229 | Okaite | CC_Spot6 | 19.77 | 0.10 | 15.71 | 0.09 | 39.35 | 0.21 | 0.7943 | 0.0011 | 1.9880 | 0.0017 |
| | | MEL_Spot6 | 19.69 | 0.06 | 15.70 | 0.06 | 39.31 | 0.13 | 0.7975 | 0.0007 | 1.9963 | 0.0013 |
| | | MEL2_Spot6 | 19.87 | 0.11 | 15.65 | 0.09 | 39.27 | 0.22 | 0.7878 | 0.0008 | 1.9762 | 0.0018 |
| Oka21 | Calcitic ijolite | CC1 | 19.17 | 0.08 | 15.38 | 0.06 | 38.24 | 0.14 | 0.8021 | 0.0009 | 1.9948 | 0.0020 |
| | | CC3 | 19.21 | 0.08 | 15.44 | 0.06 | 38.37 | 0.16 | 0.8036 | 0.0007 | 1.9961 | 0.0017 |
| | | CC3_2 | 19.17 | 0.04 | 15.36 | 0.03 | 38.23 | 0.08 | 0.8011 | 0.0004 | 1.9937 | 0.0009 |
| Oka31 | Calcitic ijolite | CC1 | 19.26 | 0.04 | 15.44 | 0.03 | 38.51 | 0.07 | 0.8019 | 0.0003 | 1.9996 | 0.0007 |
| | | CC3 | 19.20 | 0.06 | 15.40 | 0.05 | 38.45 | 0.11 | 0.8019 | 0.0005 | 2.0023 | 0.0011 |
| | | CC5 | 19.25 | 0.03 | 15.46 | 0.03 | 38.50 | 0.06 | 0.8023 | 0.0004 | 1.9986 | 0.0009 |
| | | CC6 | 19.13 | 0.04 | 15.37 | 0.03 | 38.26 | 0.08 | 0.8031 | 0.0004 | 2.0000 | 0.0009 |
| Oka89 | Calcitic ijolite | CC1 | 19.66 | 0.04 | 15.63 | 0.03 | 39.11 | 0.07 | 0.7989 | 0.0006 | 1.9890 | 0.0009 |
| | | CC4 | 19.62 | 0.11 | 15.73 | 0.09 | 39.16 | 0.22 | 0.8019 | 0.0008 | 1.9963 | 0.0024 |
| | | CC5 | 19.65 | 0.08 | 15.73 | 0.07 | 39.11 | 0.15 | 0.8013 | 0.0009 | 1.9935 | 0.0017 |
| | | CC8 | 19.67 | 0.06 | 15.76 | 0.06 | 39.21 | 0.14 | 0.8008 | 0.0008 | 1.9941 | 0.0016 |
| | | CC12 | 19.63 | 0.07 | 15.61 | 0.06 | 39.29 | 0.14 | 0.7956 | 0.0009 | 2.0013 | 0.0022 |
| | | CC_Spot1 | 19.59 | 0.05 | 15.62 | 0.04 | 38.92 | 0.09 | 0.7976 | 0.0005 | 1.9872 | 0.0010 |
| Oka73 | Alnoite | CC1 | 19.73 | 0.08 | 15.64 | 0.06 | 39.19 | 0.17 | 0.7921 | 0.0009 | 1.9834 | 0.0014 |
| | | CC3 | 19.72 | 0.06 | 15.63 | 0.05 | 39.15 | 0.14 | 0.7918 | 0.0009 | 1.9842 | 0.0013 |
| Oka75 | Alnoite | CC2 | 19.52 | 0.12 | 15.44 | 0.10 | 38.63 | 0.23 | 0.7908 | 0.0009 | 1.9824 | 0.0019 |
| Oka70 | Jacupirangite | CC1 | 19.56 | 0.06 | 15.59 | 0.03 | 38.93 | 0.10 | 0.7963 | 0.0005 | 1.9881 | 0.0011 |

**Table 1** (*continued*)

| Sample | Rock types | Analysis No. | $^{206}Pb/^{204}Pb$ | $2\sigma_{(mean)}$ | $^{207}Pb/^{204}Pb$ | $2\sigma_{(mean)}$ | $^{208}Pb/^{204}Pb$ | $2\sigma_{(mean)}$ | $^{207}Pb/^{206}Pb$ | $2\sigma_{(mean)}$ | $^{208}Pb/^{206}Pb$ | $2\sigma_{(mean)}$ |
|---|---|---|---|---|---|---|---|---|---|---|---|---|
| Oka78 | Jacupirangite | NEPH_Spot3 | 19.06 | 0.09 | 15.17 | 0.07 | 37.83 | 0.15 | 0.7944 | 0.0009 | 1.9822 | 0.0016 |
| | | NEPH2 | 19.72 | 0.07 | 15.42 | 0.05 | 39.05 | 0.13 | 0.7819 | 0.0008 | 1.9796 | 0.0022 |
| | | NEPH3 | 19.52 | 0.07 | 15.46 | 0.05 | 38.82 | 0.11 | 0.7924 | 0.0009 | 1.9897 | 0.0012 |

Note: Carb. = carbonatite; CC = calite; MEL = melilite; NEPH = nepheline.

(e.g., Condie, 1993; Vervoort and Blichert-Toft, 1999); this major chemical differentiation event was also recorded by the Sr isotope compositions of alkaline complexes in North America (Bell et al., 1982), and Hf (and Nd) isotope systematics of oceanic basalts worldwide (Vervoort and Blichert-Toft, 1999). Fig. 7b illustrates the three-stage Pb growth evolution model curves that yield the depleted $^{208}Pb/^{204}Pb$ ratios for the proposed ADM source.

The three-stage Pb evolution history for the ADM outlined above requires that it remained isolated subsequent to its enrichment at 2.7 Ga. Thus, it is possible that the ADM reservoir was subducted shortly after its enrichment within a tectonically active regime and subsequently sank to the deep mantle. In contrast, a recent study proposed that the depleted Pb isotope signatures from the MIP-related intrusions resulted from input of portions of Archean mantle residing at the base of the

**Table 2**
in-situ Sr isotope composition of calcite from Oka.

| Sample | Rock types | Analysis No. | $^{87}Sr/^{86}Sr_{corr.}$ | $2\sigma$ | $^{84}Sr/^{86}Sr_{corr.}$ | $2\sigma$ | $^{84}Sr/^{88}Sr_{corr.}$ | $2\sigma$ | $^{88}Sr$ (V) |
|---|---|---|---|---|---|---|---|---|---|
| Coral | | | 0.70910 | 0.00001 | | | | | |
| Oka51 | Carb. | CC1 | 0.70326 | 0.00006 | 0.05650 | 0.00003 | 0.00675 | 0.000003 | 11.8 |
| | | CC2 | 0.70324 | 0.00006 | 0.05643 | 0.00003 | 0.00674 | 0.000003 | 9.2 |
| | | CC4 | 0.70321 | 0.00007 | 0.05670 | 0.00005 | 0.00677 | 0.000006 | 5.3 |
| | | CC10 | 0.70321 | 0.00005 | 0.05679 | 0.00002 | 0.00678 | 0.000003 | 8.7 |
| Oka92 | Carb. | CC1 | 0.70321 | 0.00004 | 0.05637 | 0.00003 | 0.00673 | 0.000003 | 6.7 |
| | | CC4 | 0.70319 | 0.00004 | 0.05608 | 0.00004 | 0.00670 | 0.000005 | 5.1 |
| | | CC6 | 0.70324 | 0.00006 | 0.05502 | 0.00006 | 0.00657 | 0.000007 | 4.0 |
| Oka109 | Carb. | CC5 | 0.70322 | 0.00008 | 0.05666 | 0.00005 | 0.00677 | 0.000006 | 4.7 |
| | | CC8 | 0.70332 | 0.00004 | 0.05645 | 0.00002 | 0.00674 | 0.000002 | 8.7 |
| | | CC9 | 0.70322 | 0.00005 | 0.05632 | 0.00005 | 0.00673 | 0.000006 | 8.4 |
| | | CC12 | 0.70320 | 0.00005 | 0.05642 | 0.00005 | 0.00675 | 0.000005 | 9.5 |
| Oka200a | Carb. | CC2 | 0.70314 | 0.00005 | 0.05698 | 0.00004 | 0.00680 | 0.000005 | 5.4 |
| | | CC4 | 0.70327 | 0.00006 | 0.05631 | 0.00005 | 0.00672 | 0.000006 | 5.5 |
| | | CC5 | 0.70329 | 0.00005 | 0.05640 | 0.00004 | 0.00673 | 0.000004 | 7.7 |
| Oka200c | Carb. | CC2 | 0.70333 | 0.00008 | 0.05641 | 0.00003 | 0.00674 | 0.000003 | 6.7 |
| | | CC5 | 0.70324 | 0.00006 | 0.05643 | 0.00003 | 0.00674 | 0.000004 | 5.7 |
| | | CC11 | 0.70323 | 0.00005 | 0.05643 | 0.00003 | 0.00674 | 0.000003 | 8.6 |
| Oka4a | Carb. | CC5 | 0.70323 | 0.00003 | 0.05657 | 0.00001 | 0.00675 | 0.000001 | 16.3 |
| | | CC6 | 0.70323 | 0.00003 | 0.05654 | 0.00001 | 0.00675 | 0.000001 | 18.9 |
| | | CC9 | 0.70325 | 0.00005 | 0.05652 | 0.00001 | 0.00675 | 0.000002 | 20.3 |
| | | CC10 | 0.70326 | 0.00004 | 0.05649 | 0.00001 | 0.00674 | 0.000001 | 18.6 |
| | | CC11 | 0.70322 | 0.00003 | 0.05654 | 0.00001 | 0.00675 | 0.000001 | 19.7 |
| Oka4b | Carb. | CC1 | 0.70324 | 0.00004 | 0.05662 | 0.00001 | 0.00676 | 0.000001 | 27.2 |
| | | CC2 | 0.70327 | 0.00005 | 0.05657 | 0.00001 | 0.00675 | 0.000002 | 34.7 |
| | | CC3 | 0.70323 | 0.00005 | 0.05662 | 0.00001 | 0.00676 | 0.000001 | 24.2 |
| | | CC4 | 0.70322 | 0.00004 | 0.05661 | 0.00001 | 0.00676 | 0.000001 | 12.5 |
| Oka72 | Carb. | CC2 | 0.70343 | 0.00006 | 0.05642 | 0.00004 | 0.00674 | 0.000005 | 6.1 |
| | | CC4 | 0.70341 | 0.00005 | 0.05651 | 0.00003 | 0.00675 | 0.000003 | 8.3 |
| Oka153 | Carb. | CC1 | 0.70334 | 0.00002 | 0.05630 | 0.00001 | 0.00672 | 0.000001 | 19.4 |
| | | CC3 | 0.70344 | 0.00002 | 0.05630 | 0.00001 | 0.00672 | 0.000001 | 16.2 |
| | | CC4 | 0.70337 | 0.00002 | 0.05629 | 0.00001 | 0.00672 | 0.000001 | 16.0 |
| | | CC12 | 0.70336 | 0.00002 | 0.05628 | 0.00001 | 0.00672 | 0.000002 | 13.3 |
| Oka206 | Carb. | CC1 | 0.70326 | 0.00003 | 0.05663 | 0.00001 | 0.00676 | 0.000002 | 29.6 |
| | | CC2 | 0.70326 | 0.00006 | 0.05650 | 0.00003 | 0.00675 | 0.000003 | 12.2 |
| Oka203 | Carb. | CC1 | 0.70330 | 0.00004 | 0.05643 | 0.00009 | 0.00675 | 0.000011 | 17.6 |
| | | CC3 | 0.70327 | 0.00005 | 0.05645 | 0.00016 | 0.00673 | 0.000019 | 8.8 |
| Oka138 | Okaite | CC1 | 0.70332 | 0.00004 | 0.05652 | 0.00001 | 0.00675 | 0.000001 | 19.3 |
| | | CC2 | 0.70337 | 0.00003 | 0.05653 | 0.00001 | 0.00675 | 0.000001 | 19.5 |
| Oka229 | Okaite | CC2b | 0.70323 | 0.00009 | 0.05738 | 0.00001 | 0.00683 | 0.000001 | 10.5 |
| | | CC8 | 0.70328 | 0.00006 | 0.05679 | 0.00012 | 0.00677 | 0.000015 | 8.1 |
| | | CC9 | 0.70316 | 0.00007 | 0.05734 | 0.00011 | 0.00682 | 0.000013 | 6.8 |
| Oka21 | Calcitic ijolite | CC1 | 0.70325 | 0.00007 | 0.05710 | 0.00008 | 0.00682 | 0.000010 | 6.2 |
| | | CC3 | 0.70334 | 0.00008 | 0.05635 | 0.00008 | 0.00672 | 0.000010 | 8.8 |
| Oka31 | Calcitic ijolite | CC1 | 0.70331 | 0.00003 | 0.05654 | 0.00002 | 0.00676 | 0.000002 | 14.9 |
| | | CC3 | 0.70332 | 0.00003 | 0.05657 | 0.00002 | 0.00676 | 0.000002 | 16.7 |
| | | CC5 | 0.70333 | 0.00003 | 0.05659 | 0.00002 | 0.00676 | 0.000002 | 12.3 |
| Oka89 | Calcitic ijolite | CC1 | 0.70338 | 0.00006 | 0.05647 | 0.00003 | 0.00674 | 0.000004 | 10.0 |
| | | CC4 | 0.70340 | 0.00004 | 0.05654 | 0.00004 | 0.00675 | 0.000004 | 12.0 |
| | | CC12 | 0.70335 | 0.00008 | 0.05648 | 0.00004 | 0.00675 | 0.000004 | 10.0 |
| Oka75 | Alnoite | CC2 | 0.70330 | 0.00004 | 0.05649 | 0.00001 | 0.00675 | 0.000002 | 8.6 |
| | | CC3 | 0.70335 | 0.00003 | 0.05655 | 0.00002 | 0.00675 | 0.000002 | 8.6 |
| Oka70 | Jacupirangite | CC1 | 0.70314 | 0.00004 | 0.05695 | 0.00008 | 0.00679 | 0.000011 | 4 |
| | | CC2 | 0.70323 | 0.00005 | 0.05653 | 0.00011 | 0.00678 | 0.000015 | 7.5 |
| | | CC3 | 0.70324 | 0.00004 | 0.05674 | 0.00014 | 0.00669 | 0.000021 | 5.3 |

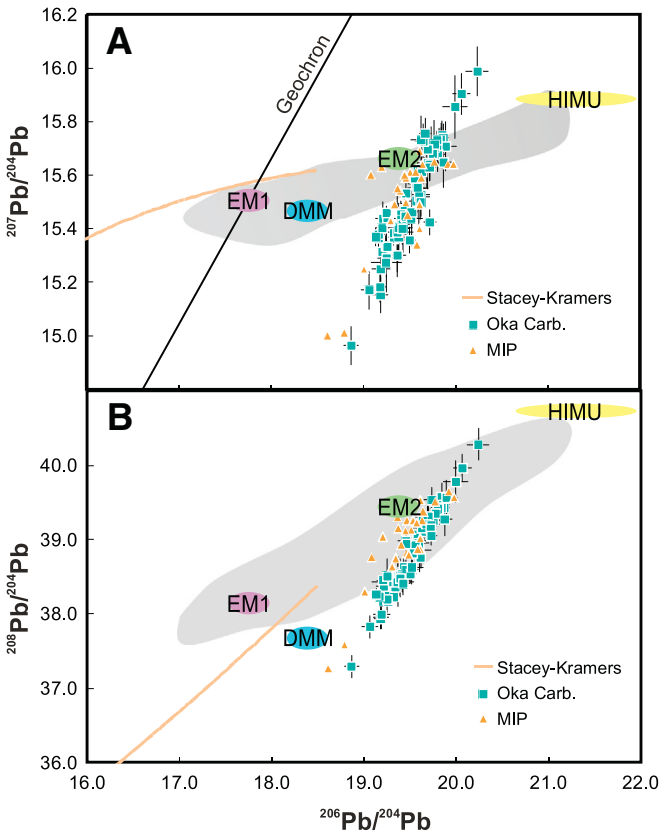


**Fig. 4.** Plots of $^{207}Pb/^{204}Pb$ vs $^{206}Pb/^{204}Pb$ (A) and $^{208}Pb/^{204}Pb$ vs $^{206}Pb/^{204}Pb$ (B) comparing the Pb isotope ratios between those for Oka and MIP-related intrusions, and young carbonatites (<200 Ma) worldwide (gray shaded area). Of note, the in-situ Pb isotopic ratios obtained here for Oka alone overlap the entire range of values for reported from MIP-related intrusions (Roulleau et al., 2012); the latter were analyzed by solution mode MC-ICP-MS (i.e., subsequent sample digestion and ion exchange chemistry) from a different laboratory (Roulleau and Stevenson, 2013; Roulleau et al., 2012). The isotopic fields for HIMU, EM1, EM2, and DMM mantle reservoirs (Zindler and Hart, 1986) are also illustrated. The 4.56 Ga Geochron is also plotted in A. Individual analyses are listed in Table 1.

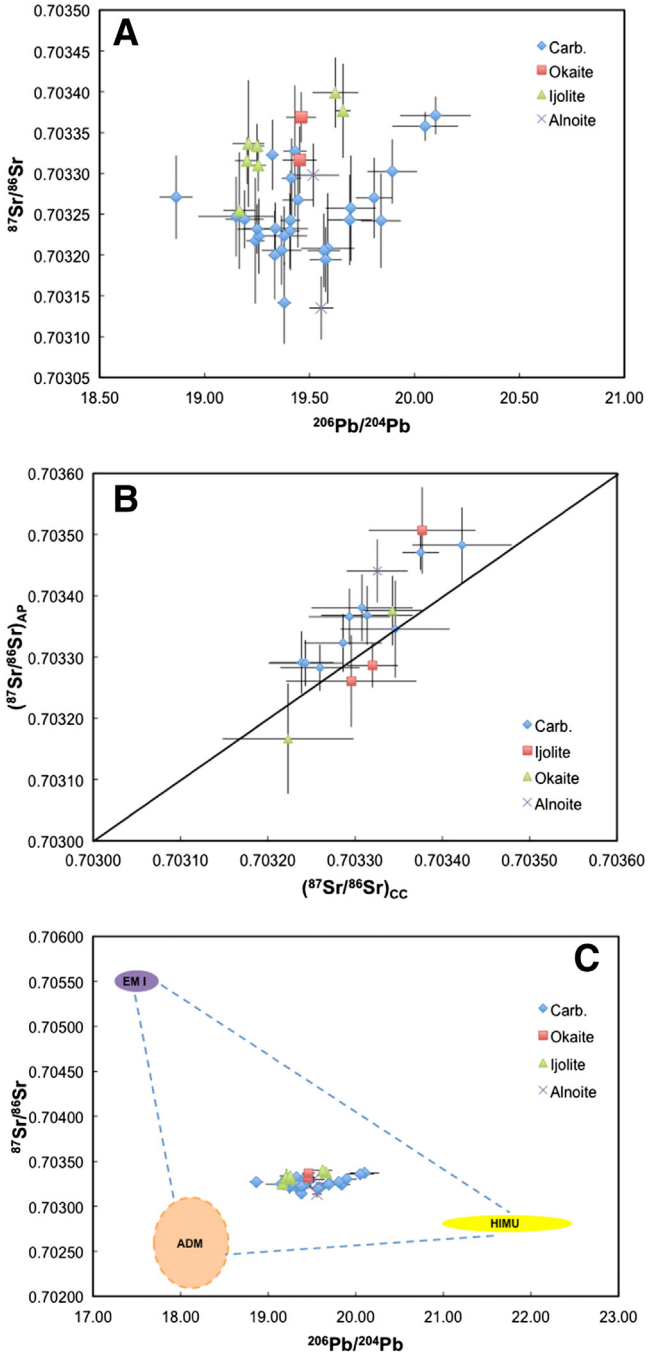


**Fig. 5.** Plots displaying the Sr and Pb isotope compositions for constituent minerals from Oka. (A) In-situ $^{87}Sr/^{86}Sr$ vs $^{206}Pb/^{204}Pb$ diagram for calcite from carbonatite, okaite and ijolite at Oka; (B) Sr isotopic ratios for calcite are compared to those for apatite from the same sample; (C) Plot of $^{87}Sr/^{86}Sr$ vs $^{206}Pb/^{204}Pb$ for analyses reported here and these are compared to isotope compositions of mantle endmembers. The Sr isotopic ratios for apatite are taken from Chen and Simonetti (2014). The isotope data presented in this figure are average ratios for a single sample. 'ADM' = ancient depleted mantle — see text for detailed explanation.

subcontinental lithosphere mantle (SCLM; Roulleau and Stevenson, 2013). Moreover, the portions of Archean mantle were restricted to the southeastern region of the MIP; however, this interpretation is inconsistent with the following critical observations reported here: 1. The depleted Pb isotope signatures from Oka suggest that input from an ADM-type component is prevalent throughout the entire geographic extent of the MIP and not just the southeastern region (Fig. 1); 2. The Pb isotope compositions for cratonic mantle peridotites (predominantly lherzolite and harzburgite) within the eastern Superior Province as sampled by the Renard Kimberlites, north-central Québec (Hunt et al., 2012), which yield a model age of ~2.7 Ga, are significantly different compared to the proposed Pb isotope signature for ADM (Fig. 7); and 3. Nd isotope ratios from apatite (from Chen and Simonetti, 2014) are depleted and do not correlate (i.e. scatter) relative to their corresponding Pb isotope ratios (i.e., relatively constant Nd isotope ratios with variable Pb isotope ratios; Fig. 8a), and hence do not define the same 'lithospheric contamination' trend as the alkaline silicate rocks related to MIP-related intrusions (Roulleau and Stevenson, 2013; Fig. 8a). As noted earlier, it is difficult to perturb the Nd and Sr isotope signatures for carbonatites obtained from their mantle source due to their inherently high abundances of these elements (1000s of ppm; e.g., Chen and Simonetti, 2013). In addition, the extremely heterogeneous and more radiogenic Pb isotope signature of subcontinental, Archean mantle peridotites in north-central Québec (Fig. 7) indicates how difficult it is for lithospheric mantle to remain chemically and isotopically (for Pb) "closed" over billions of years. This also argues against the existence (and preservation) of an ADM-type source within the SCLM in NE North America. In contrast, based on the most radiogenic $^{186}Os/^{188}Os$ ratios recorded for lavas at Loihi and Hualalai (Hawaii), Brandon et al. (1999) have shown that preservation/isolation and sampling of ancient recycled crustal components by a deep (core–mantle boundary) plume is entirely plausible. Moreover, Bizzarro et al. (2002) argue for the existence of an ancient (>3.0 Ga old) 'radiogenic' mantle component present in the deep mantle based on the Hf isotope composition of carbonatite/kimberlite complexes in Greenland and South Africa.

### 5.2. Crustal contamination

Isotope variations in many continental igneous rocks may be attributed to crustal contamination processes, and it was proposed by Grünenfelder et al. (1986) and Roulleau et al. (2012) to explain some of the isotopic heterogeneity at Oka and MIP-related intrusions, respectively. Given the additional radiogenic and stable isotope data obtained in this study, the crustal contamination hypothesis can now be more thoroughly evaluated for Oka: 1) O and C isotope compositions reported here are indicative of derivation from mantle sources (Fig. 6, Table 3), and are not consistent with the involvement of crustal materials. Furthermore, the stable C and O isotope values do not support the arguments relating the radiogenic Sr and Pb isotope variations to hydrothermal (post solidification) alteration. The latter typically produces 'heavier' $\delta^{13}C$ and $\delta^{18}O$ values that plot outside of the primary mantle box (Fig. 6; e.g., Denies, 1989). 2) Carbonatites contain higher Sr and Nd contents compared to their associated silicate rocks, and therefore, their corresponding Sr and Nd isotope signatures are most likely pristine and least affected (if at all) by crustal contamination. However, the radiogenic isotope compositions of carbonatites indicate a larger variation compared to the associated silicate rocks (Fig. 5), and it is therefore difficult to attribute this discrepancy to crustal contamination; 3) The Oka-MIP linear Pb–Pb isotope arrays are far removed from both the Pb isotope field for lower crustal rocks from the proximal Grenville Province (Gariépy and Verner, 1990) and the Stacey and Kramers' Pb evolution line, which is interpreted to represent the time-integrated Pb isotopic compositions for average continental crust (Fig. 7; Stacey and Kramers, 1975). Hence, we believe that crustal contamination did not play a role in contributing to the radiogenic and stable isotopic variations for the rocks investigated here from Oka.

### 5.3. Petrogenetic history of the Oka carbonatite complex

As discussed above, the radiogenic (Sr, Nd, Pb) and stable (C and O) isotope compositions for both carbonatite and the associated silicate rocks (i.e., okaite, calcitic ijolite, ijolite, alnoite and jacupirangite) define a similar range of values. The similar isotope ratios between these two rock groups (carbonatites and silicates) may be consistent with magmatic differentiation processes such as liquid immiscibility, or the melting of the same isotopically heterogeneous mantle source region.

Chen and Simonetti (2013) report the major and trace element chemistry of calcite and apatite from carbonatite and okaite, and these define a wide range of values, in particular for the trace elements. On the basis of the mineral trace element compositions for both apatite and calcite, Chen and Simonetti (2013) attempted to model the abundances of La and Ce by both equilibrium and fractional crystallization processes. Using available partition coefficients for these two elements within carbonate and apatite igneous systems and assuming various plausible parental melt compositions, Chen and Simonetti (2013) were unable to reproduce both the range and extent of the La and Ce compositions. Moreover, the in-situ U–Pb ages for apatite indicate a protracted crystallization history that occurred between ~127 and ~115 Ma ago. Hence, the combined major and trace element data, and U–Pb geochronological results clearly indicate that apatite and calcite at Oka formed in complex igneous system that most probably involved continuous generation of small volume melts from a recently metasomatized mantle source region (Chen and Simonetti, 2013). The complicated crystallization history for the complex is corroborated by the complexly zoned patterns for apatite as revealed by cathodoluminescence imagery (Chen and Simonetti, 2013), and the bimodal U–Pb ages for niocalite within individual samples (Chen et al., 2013b). The latter feature suggests that some of the niocalite crystals represent earlier-formed, cognate crystals that were scavenged by later melts within the mantle source region for Oka (Chen et al., 2013b). In summary, the petrogenetic history for Oka is far from being simple since it involves more than one parental melt, being generated from an isotopically heterogeneous mantle source over a period of ~10 to ~15 Ma.

Fig. 8b further corroborates the complexity of the igneous system at Oka since the Pb isotope compositions for calcite do not correlate with their corresponding REE contents, which clearly rules out the possibility of melt differentiation processes occurring within a closed system, such as liquid immiscibility. The fact that REE (total) abundances for calcite tend to be higher for analyses characterized by less radiogenic Pb isotope compositions (Fig. 8b) indicates that the trace element enrichment/metasomatism of the mantle source is a recent event and most likely occurred just prior to melt formation. In addition, the variable $\delta^{13}C$ values at relatively constant oxygen isotope values (Fig. 6) cannot be solely attributed to melt differentiation processes, such as fractional crystallization (Denies, 1989).

Our preferred interpretation for explaining the radiogenic and stable isotope systematics of the Oka carbonatites and associated alkaline silicate rocks from the MIP involves several mantle sources, which includes a mantle plume that is characterized by a mixed HIMU–EM1 signature. A similar model has been proposed for carbonatitic and alkaline magmatic activity associated with the East African Rift (e.g., Bell and Simonetti, 2010; Bell and Tilton, 2001). Griffiths and Campbell (1990) argued that it is possible to entrain ambient mantle during the ascent of thermal plumes because of coupling between heat conduction and laminar stirring driven by plume motion. Hence, we propose that the HIMU–EM1 plume giving rise to Oka and MIP-related alkaline activity

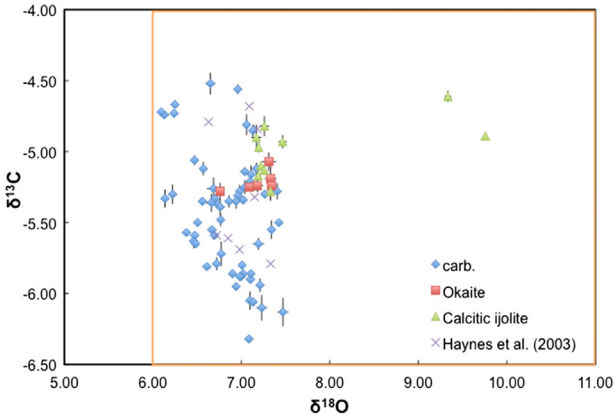


**Fig. 6.** Shown are C and O isotopic compositions for individual calcite crystals from carbonatite, okaite and ijolite. Data from Haynes et al. (2003) and the 'mantle box' (in orange; Keller and Hoefs, 1995) are also shown. (For interpretation of the references to color in this figure legend, the reader is referred to the web version of this article.)

**Table 3**
C and O isotopic compositions for calcite from Oka.

| Sample | Rock types | $\delta^{18}O$ (‰) | σ | $\delta^{13}C$ (‰) | σ |
|---|---|---|---|---|---|
| Oka51 | Carb. | 7.16 | 0.03 | −5.42 | 0.06 |
| Oka92 | Carb. | 7.26 | 0.04 | −5.35 | 0.03 |
| Oka109 | Carb. | 6.59 | 0.03 | −5.71 | 0.05 |
| Oka200a | Carb. | 6.52 | 0.03 | −5.09 | 0.04 |
| Oka200b | Carb. | 6.64 | 0.04 | −5.45 | 0.04 |
| Oka200c | Carb. | 6.83 | 0.05 | −5.44 | 0.06 |
| Oka4a | Carb. | 7.11 | 0.03 | −6.14 | 0.04 |
| Oka4b | Carb. | 6.44 | 0.03 | −5.60 | 0.01 |
| Oka72 | Carb. | 7.11 | 0.05 | −5.65 | 0.05 |
| Oka144 | Carb. | 7.03 | 0.04 | −5.88 | 0.03 |
| Oka153 | Carb. | 6.88 | 0.03 | −5.77 | 0.02 |
| Oka203 | Carb. | 6.71 | 0.06 | −5.65 | 0.06 |
| Oka206 | Carb. | 6.76 | 0.04 | −5.84 | 0.02 |
| Oka137 | Okaite | 7.20 | 0.41 | −5.16 | 0.04 |
| Oka138 | Okaite | 7.05 | 0.05 | −5.24 | 0.07 |
| Oka229 | Okaite | 7.26 | 0.05 | −5.24 | 0.05 |
| Oka21 | Calcitic ijolite | 7.47 | 0.04 | −4.81 | 0.03 |
| Oka31 | Calcitic ijolite | 7.19 | 0.03 | −5.04 | 0.04 |
| Oka89 | Calcitic ijolite | 7.28 | 0.04 | −5.08 | 0.05 |

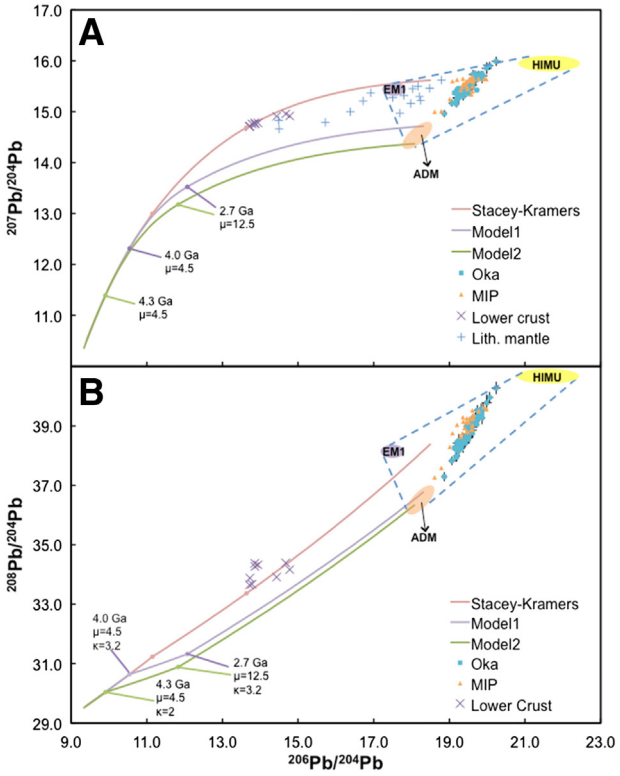


**Fig. 7.** $^{207}Pb/^{204}Pb$ (A) and $^{208}Pb/^{204}Pb$ (B) vs $^{206}Pb/^{204}Pb$ diagrams. Both illustrate the multi-stage Pb growth evolution models proposed to explain the Pb isotope composition for the ADM (see text for details). Also illustrated are the Stacey and Kramers (1975) Pb evolution model, the Pb isotope composition of proximal lower crustal rocks from the Grenville Province, Québec (Gariépy and Verner, 1990), the Pb isotope composition for ~2.7 Ga old cratonic mantle peridotites, north-central Québec (Hunt et al., 2012), and two mantle components (HIMU and EM1; Zindler and Hart, 1986). Modeling parameters are discussed in detail in the text.

entrained ADM material during its ascent from the deep mantle through the overlying mantle and crust.

The HIMU–EM1 plume material intermingled with the ADM during the prolonged magmatism (over ~15 million years; Chen and Simonetti, 2014) associated with the MIP-related intrusions, which resulted in generating the linear Pb–Pb isotope arrays. Alternatively, it is possible that the ADM represents lower mantle material (i.e., at the core–mantle boundary — CMB) and the enriched components (EM1 and HIMU) are entrained during the ascent of a plume. Interestingly, the constituent minerals from Oka most characterized by the ADM depleted Pb isotope 'signature' contain relatively lighter $\delta^{13}C$ isotopic ratios (Fig. 8c). Isotopically lighter carbon present within magmatic/mantle systems may be linked either to organic matter introduced within Earth's mantle via the subduction of oceanic crust (and lithosphere), or represents primordial heterogeneities preserved in the Earth's interior (Cartigny et al., 2001; Deines et al., 2001; Shirey et al., 2013; Smart et al., 2011). It is obvious that the $\delta^{13}C$ values reported here are not significantly depleted so as to indicate (unequivocally) the input of organic-derived carbon, which is typically characterized by 'light' $\delta^{13}C$ values (<−30‰); more importantly, Fig. 8c shows the positive correlation between $\delta^{13}C$ values and Pb isotope ratios, which is consistent with our interpretation, and hence does not argue against input from recycled crustal material.

The detailed Pb isotope study of lavas from the volcanic chains of Mauna Loa and Mauna Kea (Hawaii) demonstrate large-scale heterogeneities, and these also define distinct linear arrays in Pb–Pb isotope plots (Abouchami et al., 2005). On the basis of the overall consistency of the Pb isotopic signatures shown by the Mauna Loa and Mauna Kea chains, Abouchami et al. (2005) suggest that the Hawaiian plume is characterized by a gross lateral zonation. The latter model is consistent with the

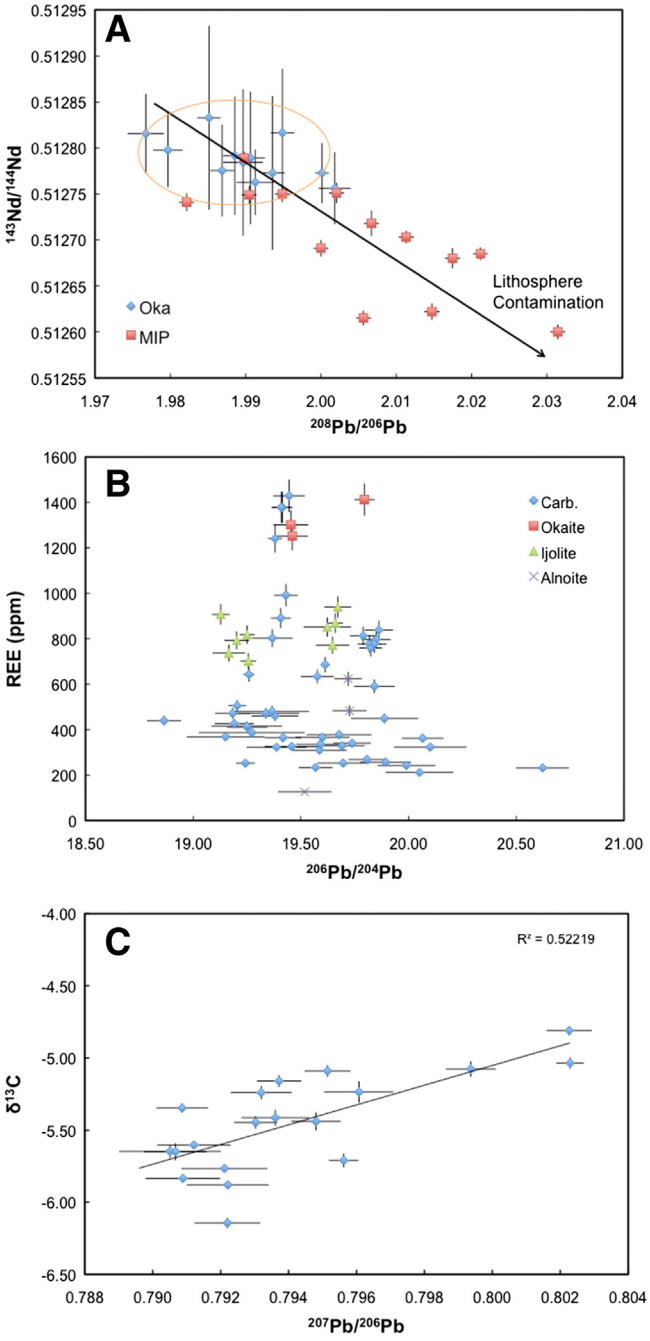


**Fig. 8.** Plots of $^{143}Nd/^{144}Nd$ vs $^{208}Pb/^{206}Pb$ (A), $^{206}Pb/^{204}Pb$ vs REE contents (B), and $\delta^{13}C$ vs $^{207}Pb/^{206}Pb$ (C). $\delta^{13}C$ values for calcite from Oka overlap those for mantle-derived carbonate (Bell and Simonetti, 2010; Eby, 1985), and Nd isotopes for Oka are taken from Chen and Simonetti (2014). Nd and Pb isotope data for MIP-related intrusions are from Roulleau and Stevenson (2013).

numerical simulations of plume evolution (Farnetani et al., 2002), which indicate that plumes draw compositional heterogeneities from a low-viscosity source layer into the plume stem by laminar flow. Thus, this process should preserve any incidental, lateral, initial heterogeneities of the source layer, which perhaps is located above the core–mantle boundary and may contain large-scale (100s km) heterogeneities (Kellogg et al., 1999). These are then pulled into, compressed and vertically stretched within the plume stem. Moreover, Kumagai (2002) conducted experiments involving laminar entrainment of mantle plumes with compositional buoyancy, and determined that the resulting structure is a function of the viscosity ratio (defined as the ratio of the ambient mantle to the buoyant fluid). At low viscosity ratios,

a vortex ring structure is produced in which the plumes entrain the ambient fluids and form a rotating multi-layered structure within their heads. This type of layered structure is most likely to preserve initial elemental and isotopic compositions (Kumagai, 2002). Alternatively, plume entrainment at higher viscosity ratios results in chaotic stirring and hence is more likely to produce a more homogeneous (chemical and isotopic) plume head. Thus, the combined results of laminar flow experiments/simulations and Pb isotope systematics from Hawaiian volcanic chains indicate that it is possible for mantle plumes to sample and preserve deep-seated (e.g., core–mantle boundary) heterogeneous isotope domains/components.

## 6. Conclusions

The Sr, Nd, Pb, C, and O isotope ratios reported here for constituent minerals contained within both carbonatites and associated silicate rocks from Oka are variable and cannot be produced by either partial melting of an isotopically homogeneous mantle source, or closed-system differentiation of solely one parental magma. The isotope variations are most likely the result of mixing of discrete, small volume mantle melts derived from an isotopically heterogeneous plume source. In particular, the mantle plume has sampled and entrained a deep-seated, ancient, isotopically depleted mantle component (ADM) that is present throughout the entire length and duration of the MIP-related magmatism. Crustal contamination can be effectively ruled out in the petrogenetic history of the Oka carbonatites and associated alkaline silicate rocks based on the combined radiogenic (Sr, Pb, and Nd) and stable (C and O) isotope data reported in this study.

## Acknowledgments

The authors thank Sandy Dillard from Brazos Petrographic Thin Section Services for thin section preparation. W. Chen received financial support from the University of Notre Dame during her doctoral dissertation work. Comments and suggestions provided by Lucy Hunt and an anonymous reviewer are greatly appreciated.

## References

Abouchami, W., Hofmann, A.W., Galer, S.J.G., Frey, F.A., Eisele, J., Feigenson, M., 2005. Lead isotopes reveal bilateral asymmetry and vertical continuity in the Hawaiian mantle plume. Nature 434, 851–856.

Andersen, T., Taylor, P.N., 1988. Pb isotope chemistry of the Fen carbonatite complex, S.E. Norway: age and petrogenetic implications. Geochimica et Cosmochimica Acta 52, 209–215.

Balaganskaya, E.G., Downes, H., Demaiffe, D., 2007. REE and Sr–Nd isotope compositions of clinopyroxenites, phoscorites, and carbonatites of the Seblyavr Massif, Kola Peninsula, Russa. Mineralogia Polonica 38, 29–45.

Baker, J., Peate, D., Waight, T., Meyzen, C., 2004. Pb isotopic analysis of standards and samples using a $^{207}Pb$–$^{204}Pb$ double spike and thallium to correct for mass bias with a double-focusing MC-ICP-MS. Chemical Geology 211, 275–303.

Bell, K., 1998. Radiogenic isotope constraints on relationships between carbonatites and associated silicate rocks — a brief review. Journal of Petrology 39, 1987–1996.

Bell, K., Simonetti, A., 1996. Carbonatite magmatism and plume activity: implications from the Nd, Pb and Sr isotope systematics of Oldoinyo Lengai. Journal of Petrology 37, 1321–1339.

Bell, K., Simonetti, A., 2010. Source of parental melts to carbonatites-critical isotopic constraints. Mineralogy and Petrology 98, 77–89.

Bell, K., Tilton, G.R., 2001. Nd, Pb and Sr isotopic compositions of East African carbonatites: evidence for mantle mixing and plume inhomogeneity. Journal of Petrology 42, 1927–1945.

Bell, K., Blenkinsop, J., Cole, T.J.S., Menagh, D.P., 1982. Evidence from Sr isotopes for long-lived heterogeneities in the upper mantle. Nature 298, 251–253.

Bellucci, J.J., Simonetti, A., Wallace, C., Koeman, E.C., Burns, P.C., 2013. The Pb isotopic composition of trinitite melt glass: evidence for the presence of Canadian industrial Pb in the first atomic weapon test. Analytical Chemistry 85, 7588–7593.

Bizimis, M., Salters, V.J.M., Dawson, J.B., 2003. The brevity of carbonatite sources in the mantle, evidence from Hf isotopes. Contributions to Mineralogy and Petrology 145, 281–300.

Bizzarro, M., Simonetti, A., Stevenson, R.K., David, J., 2002. Hf isotope evidence for a hidden mantle reservoir. Geology 30, 771–774.

Bizzarro, M., Simonetti, A., Stevenson, R.K., Kurszlaukis, S., 2003. In situ $^{87}Sr/^{86}Sr$ investigation of igneous apatites and carbonates using laser ablation MC-ICP-MS. Geochimica et Cosmochimica Acta 67, 289–302.

Brandon, A.D., Norman, M.D., Walker, R.J., Morgan, J.W., 1999. $^{186}Os$–$^{187}Os$ systematics of Hawaiian picrites. Earth and Planetary Science Letters 174, 25–42.

Brassinnes, S., Balaganskaya, E., Demaiffe, D., 2005. Magmatic evolution of the differentiated ultramafic, alkaline and carbonatite intrusion of Vuoriyarvi (Kola Peninsula, Russia), a LA-ICP-MS study of apatite. Lithos 85, 76–92.

Cartigny, P., Harris, J.W., Javoy, M., 2001. Diamond genesis, mantle fractions and mantle nitrogen content: a study of $\delta^{13}C$–N concentrations in diamonds. Earth and Planetary Science Letters 185, 85–98.

Chen, W., Simonetti, A., 2013. In-situ determination of major and trace elements in calcite and apatite, and U–Pb ages of apatite from the Oka carbonatite complex: insights into a complex crystallization history. Chemical Geology 353, 151–172.

Chen, W., Simonetti, A., 2014. Evidence for the multi-stage petrogenetic history of the Oka carbonatite complex (Québec, Canada) as recorded by perovskite and apatite. Minerals 4, 437–476.

Chen, W., Kamenetsky, V., Simonetti, A., 2013a. Evidence for the alkaline nature of parental carbonatite melts at Oka complex in Canada. Nature Communications 4, 2687. http://dx.doi.org/10.1038/ncomms3687.

Chen, W., Simonetti, A., Burns, P.C., 2013b. A combined geochemical and geochronological investigation of niocalite from the Oka carbonatite complex, Canada. The Canadian Mineralogist 51, 785–800.

Collerson, K.D., Campbell, L.M., Weaver, B.L., Palacz, Z.A., 1991. Evidence for extreme mantle fractionation in early Archaean ultramafic rocks from northern Labrador. Nature 349, 209–214.

Condie, K.C., 1993. Chemical composition and evolution of the upper continental crust — contrasting results from surface samples and shales. Chemical Geology 104, 1–37.

Coplen, T.B., Kendall, C., Hopple, J., 1983. Comparison of stable isotope reference samples. Nature 302, 236–238.

Coplen, T.B., Brand, W.A., Gehre, M., Gröning, M., Meijer, H.A.J., Toman, B., Verkouteren, R.M., 2006. New guidelines for $\delta^{13}C$ measurements. Analytical Chemistry 78, 2439–2441.

Craig, 1961. Isotopic variations in meteoric waters. Science 133, 1833–1834.

Deines, P., Viljoen, F., Harris, J.W., 2001. Implications of the carbon isotope and mineral inclusion record for the formation of diamonds in the mantle underlying a mobile belt: Venetia, South Africa. Geochimica et Cosmochimica Acta 65, 813–838.

Denies, P., 1989. Stable isotope variations in carbonatites. In: Bell, K. (Ed.), Carbonatites: Genesis and evolution. Unwin Hyman, London, pp. 301–359.

Dupré, B., Allègre, C.J., 1980. Pb–Sr–Nd isotopic correlation and the chemistry of the North Atlantic mantle. Nature 286, 17–22.

Eby, G.N., 1985. Age relations, chemistry, and petrogenesis of mafic alkaline dikes from the Monteregian Hills and younger White Mountain igneous provinces. Canadian Journal of Earth Sciences 22, 1103–1111.

Farnetani, C.G., Legras, B., Tackley, P.J., 2002. Mixing and deformations in mantle plumes. Earth and Planetary Science Letters 196, 1–15.

Faure, S., Trembly, A., Angelier, J., 1996. State of intraplate stress and tectonism of northeastern America since Cretaceous times, with particular emphasis on the New England-Québec igneous province. Tectonophysics 255, 111–134.

Foland, K.A., Jiang-feng, C., Gilbert, L.A., Hofmann, A.W., 1988. Nd and Sr isotopic signatures of Mesozoic plutons in northeastern North America. Geology 16, 684–687.

Gariépy, C., Verner, D., 1990. Dating Archean metamorphic minerals southeast of the Grenville front, western Québec, using Pb isotopes. Geology 18, 1078–1081.

Gold, D.P., Eby, G.N., Bell, K., Vallée, M., 1986. Carbonatites, diatremes and ultra-alkaline rocks in the Oka area, Québec. Geological Association of Canada Guidebook 21.

Griffiths, R.W., Campbell, I.H., 1990. Stirring and structure in mantle starting plumes. Earth and Planetary Science Letters 99, 77–78.

Grünenfelder, M.H., Tilton, G.R., Bell, K., Blenkinsop, J., 1986. Lead and strontium isotope relationships in the Oka carbonatite complex, Québec. Geochimica et Cosmochimica Acta 58, 461–468.

Gulson, B.L., 1984. Uranium–lead and lead–lead investigations of minerals from the Broken Hill lodes and mine sequence rocks. Economic Geology 79, 476–490.

Halliday, A.N., Davies, G.R., Lee, D., Tommasini, S., Paslick, C.R., Fitton, J.G., James, D.E., 1992. Lead isotope evidence for young trace element enrichment in the oceanic upper mantle. Nature 359, 623–627.

Hanan, B.B., Graham, D.W., 1996. Lead and helium isotope evidence from oceanic basalts for a common deep source of mantle plumes. Science 272, 991–995.

Hart, S.R., Hauri, E.H., Oschmann, L.A., Whitehead, L.A., 1992. Mantle plumes and entrainment: isotope evidence. Science 256, 517–519.

Haynes, E.A., Moecher, D.P., Spicuzza, M.J., 2003. Oxygen isotope composition of carbonates, silicates, and oxides in selected carbonatites: constraints on crystallization temperatures of carbonatite magmas. Chemical Geology 193, 43–57.

Heaman, L.M., Kjarsgaard, B.A., 2000. Timing of eastern North American kimberlite magmatism: continental extension of the Great Meteor hotspot track? Earth and Planetary Science Letters 178, 253–268.

Hoernle, K., Tilton, G., Le Bas, M.J., Duggen, S., Garbe-Schönberg, 2002. Geochemistry of oceanic carbonatites compared with continental carbonatites: mantle recycling of oceanic crustal carbonate. Contributions to Mineralogy and Petrology 142, 520–542.

Hofmann, A.W., 1997. Mantle geochemistry: the message from oceanic volcanism. Nature 385, 219–229.

Hunt, L., Stachel, T., Grütter, H., Armstrong, J., McCandless, T.E., Simonetti, A., Tappe, S., 2012. Small mantle fragments from the Renard Kimberlites, Québec: powerful recorders of mantle lithosphere formation and modification beneath the Eastern Superior Craton. Journal of Petrology 53, 1597–1635.

Ivanikov, V.V., Rukhlov, A.S., Bell, K., 1998. Magmatic evolution of the melilitite–carbonatite–nephelinite dykes series of the Turiy Peninsula (Kandalaksha Bay, White Sea, Russia). Journal of Petrology 39, 2043–2059.

Kalt, A., Hegner, E., Satir, M., 1997. Nd, Sr, and Pb isotopic evidence for diverse lithospheric mantle sources of East African Rift carbonatites. Tectonophysics 278, 31–45.
Keller, J., Hoefs, J., 1995. Stable isotope characteristics of recent natrocarbonatites from Oldoinyo Lengai. In: Bell, K., Keller, J. (Eds.), Carbonatite Volcanism: Oldoinyo Lengai and the Petrogenesis of Natrocarbonatites 4. Springer, Berlin, pp. 113–123.
Kellogg, L.H., Hager, B.H., van der Hilst, R.D., 1999. Compositional stratification in the deep mantle. Science 283, 1881–1884.
Kramm, U., 1994. Isotope evidence for ijolite formation by fenitization — Sr–Nd data of ijolites from the type locality Iivaara, Finland. Contributions to Mineralogy and Petrology 115, 279–286.
Kumagai, I., 2002. On the anatomy of mantle plumes: effect of the viscosity ratio on entrainment and stirring. Earth and Planetary Science Letters 198, 211–224.
Kwon, S.T., Tilton, G.R., Grünenfelder, M.H., 1989. Lead isotope relationships in carbonatites and alkalic complexes: an overview. In: Bell, K. (Ed.), Carbonatites: Genesis and Evolution. Unwin Hyman, London, pp. 360–387.
McCrea, J.M., 1950. The isotopic chemistry of carbonates and a paleo-temperature scale. The Journal of Chemical Physics 18, 849–857.
Olafsson, M., Eggler, D.H., 1983. Phase relations of amphibole, amphibole–carbonate, and phlogopite–carbonate peridotite: petrologic constraints on the asthenosphere. Earth and Planetary Science Letters 64, 305–315.
Paslick, C., Halliday, A., James, D., Dawson, J.B., 1995. Enrichment of the continental lithosphere by OIB melts—isotopic evidence from the volcanic province of northern Tanzania. Earth and Planetary Science Letters 130, 109–126.
Paton, C., Woodhead, J.D., Hergt, J.M., Phillips, D., Shee, S., 2007. Strontium isotope analysis of groundmass perovskite via LA-MC-ICP-MS. Geostandards and Geoanalytical Research 31, 321–330.
Ramos, F.C., Wolf, J.A., Tollstrup, D.L., 2004. Measuring $^{87}Sr/^{86}Sr$ variations in minerals and groundmass from basalts using LA-MC-ICP-MS. Chemical Geology 211, 135–158.
Ray, J.S., Martin, M.W., Veizer, J., Bowring, S.A., 2002. U–Pb zircon dating and Sr isotope systematics of the Vindhyan Supergroup, India. Geology 30, 131–134.
Roulleau, E., Stevenson, R., 2013. Geochemical and isotopic (Nd–Sr–Hf–Pb) evidence for a lithospheric mantle source in the formation of the alkaline Monteregian Province (Québec). Canadian Journal of Earth Sciences 50, 650–666.
Roulleau, E., Pinti, D.L., Stevenson, R.K., Takahata, N., Sano, Y., Petre, F., 2012. Ar, and Pb isotopic co-variations in magmatic minerals: discriminating fractionation processes from magmatic sources in Monteregian Hills, Québec, Canada. Chemical Geology 326–327, 123–131.
Schmidberger, S.S., Simonetti, A., Heaman, L.M., Creaser, R.A., Whiteford, S., 2007. Lu–Hf, in-situ Sr and Pb isotope and trace element systematics for mantle eclogites from the Diavik diamond mine: evidence for Paleoproterozoic subduction beneath the Slave craton, Canada. Earth and Planetary Science Letters 254, 55–68.
Shields, G., Veizer, J., 2001. Precambrian seawater isotopic record. Workshop on Geochemical Reference Model. LaJolla, California, pp. 50–52.
Shirey, S.B., Cartigny, P., Frost, D.J., Keshav, S., Nestola, F., Nimis, P., Pearson, D.G., Sobolev, N.V., Walter, M.J., 2013. Diamonds and the geology of mantle carbon. Reviews in Mineralogy and Geochemistry 75, 355–421.
Simonetti, A., Bell, K., 1994. Isotopic and geochemical investigation of the Chilwa island carbonatite complex, Malawi: evidence for a depleted mantle source region, liquid immiscibility, and open-system behavior. Journal of Petrology 35, 1597–1621.
Smart, K.A., Chacko, T., Stachel, T., Muehlenbachs, K., Stern, R.A., Heaman, L.M., 2011. Diamond growth from oxidized carbon sources beneath the Northern Slave Craton, Canada: A $\delta^{13}C$-N study of eclogite-hosted diamonds from the Jericho kimberlite. Geochimica et Cosmochimica Acta 75, 6027–6047.
Stacey, J.S., Kramers, J.D., 1975. Approximation of terrestrial lead isotope evolution by a two-stage model. Earth and Planetary Science Letters 26, 207–221.
Tappe, S., Foley, S.F., Stracke, A., Romer, R.L., Kjarsgaard, B.A., Heaman, L.M., Joyce, N., 2007. Craton reactivation on the Labrador Sea margins: $^{40}Ar/^{39}Ar$ age and Sr–Nd–Hf–Pb isotope constraints from alkaline and carbonatite intrusives. Earth and Planetary Science Letters 256, 433–454.
Tilton, G.R., Bell, K., 1994. Sr–Nd–Pb isotope relationships in late Archean carbonatites and alkaline complexes: applications to the geochemical evolution of Archean mantle. Geochimica et Cosmochimica Acta 58, 3145–3154.
Tilton, G.R., Kwon, S.T., Frost, D.M., 1987. Isotopic relationships in Arkansas cretaceous alkalic complexes. In: Morris, E.M., Pasteris, J.D. (Eds.), Mantle Metasomatism and Alkaline Magmatism. Geological Society of America Special Paper 215, pp. 241–248.
Toyoda, K., Horiuchi, H., Tokonami, M., 1994. Dupal anomaly of Brazilian carbonatites: geochemical correlations with hotspots in the South Atlantic and implications for the mantle source. Earth and Planetary Science Letters 126, 315–331.
Treiman, A.H., 1989. Carbonatite magma: properties and processes. In: Bell, K. (Ed.), Carbonatites: Genesis and Evolution. Unwin Hyman, London, pp. 89–104.
Treimain, A.H., Essene, E.J., 1985. The Oka carbonatite complex, Quebec: geology and evidence for silicate-carbonate liquid immiscibility. American Mineralogist 70, 1101–1113.
Vervoort, J.D., Blichert-Toft, J., 1999. Evolution of the depleted mantle: Hf isotope evidence from juvenile rocks through time. Geochimica et Cosmochimica Acta 63, 533–556.
Wen, J., Bell, K., Blenkinsop, J., 1987. Nd and Sr isotope systematics of the Oka complex, Québec, and their bearing on the evolution of the sub-continental upper mantle. Contributions to Mineralogy and Petrology 97, 433–437.
Xu, C., Taylor, R.N., Kynicky, J., Chakhmouradian, A.R., Song, W., Wang, L., 2011. The origin of enriched mantle beneath North China block: evidence from young carbonatites. Lithos 127, 1–9.
Zindler, A., Hart, S.R., 1986. Chemical dynamics. Annual Review of Earth and Planetary Sciences 14, 493–571.
Zurevinski, S.E., Heaman, L.M., Creaser, R.A., 2011. The origin of Triassic/Jurassic kimberlite magmatism, Canada: two mantle sources revealed from the Sr–Nd isotopic composition of groundmass perovksite. Geochemistry, Geophysics, Geosystems 12. http://dx.doi.org/10.1029/2011GC003659.